

Supplementary Materials for  
**Structural insights into the formation of repulsive netrin guidance complexes**

Jessica M. Priest *et al.*

Corresponding author: Engin Özkan, [eozykan@uchicago.edu](mailto:eozykan@uchicago.edu)

*Sci. Adv.* **10**, eadj8083 (2024)  
DOI: 10.1126/sciadv.adj8083

**This PDF file includes:**

Figs. S1 to S9  
Tables S1 to S5

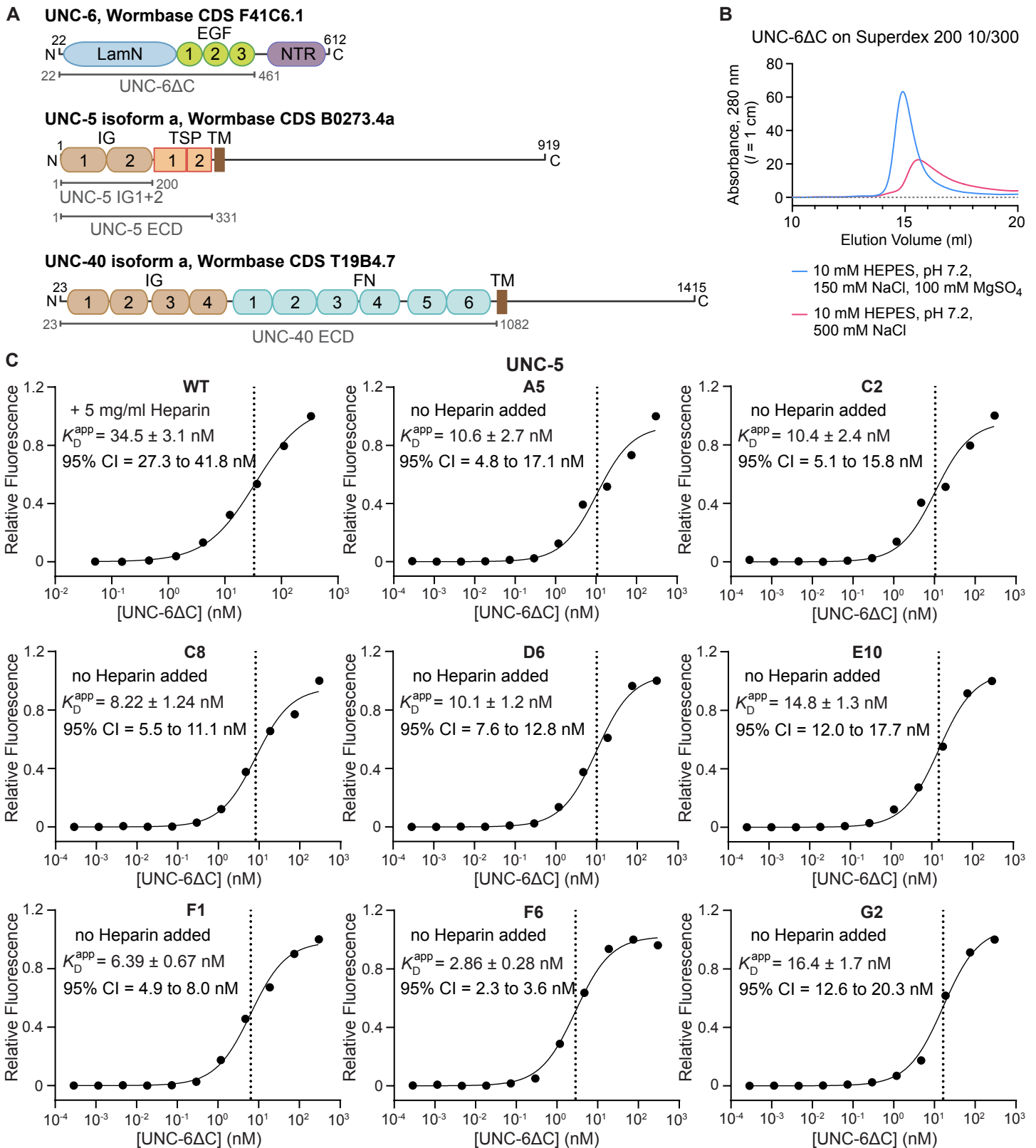


**Fig. S1. Soluble UNC-6ΔC can be used to measure binding to UNC-5 displayed and evolved on yeast.**

**A.** Schematic for boundaries of constructs used for binding studies, crystallography, biophysics, and directed evolution.

**B.** Size-exclusion chromatograms of hexahistidine-tagged UNC-6ΔC run in HBS (red), HBS containing 500 mM NaCl (blue), and HBS-MS (green). The column is a Superdex 200 10/300 (GE Healthcare). UV pathlength is 1 cm. 100 μg was loaded in both runs: The run with HBS-MS buffer recovered 89.8 μg as measured by the area under the peak (76.11 mAU×ml), while the run with high-NaCl HBS showed stronger signs of non-specific stickiness to the resin, allowing for 66.4 μg to be recovered (area = 56.25 mAU×ml). Abs-0.1% value (absorbance at 1 mg/ml) used for UNC-6ΔC is 0.845.

**C.** Binding isotherms for UNC-6ΔC to yeast expressing WT UNC-5 ECD in the presence of 5 μg/ml heparin and to eight yeast colonies expressing UNC-5 ECD variants without added heparin. Both standard errors of the non-linear fitting and the 95% confidence intervals (CI) for apparent dissociation constants are reported.

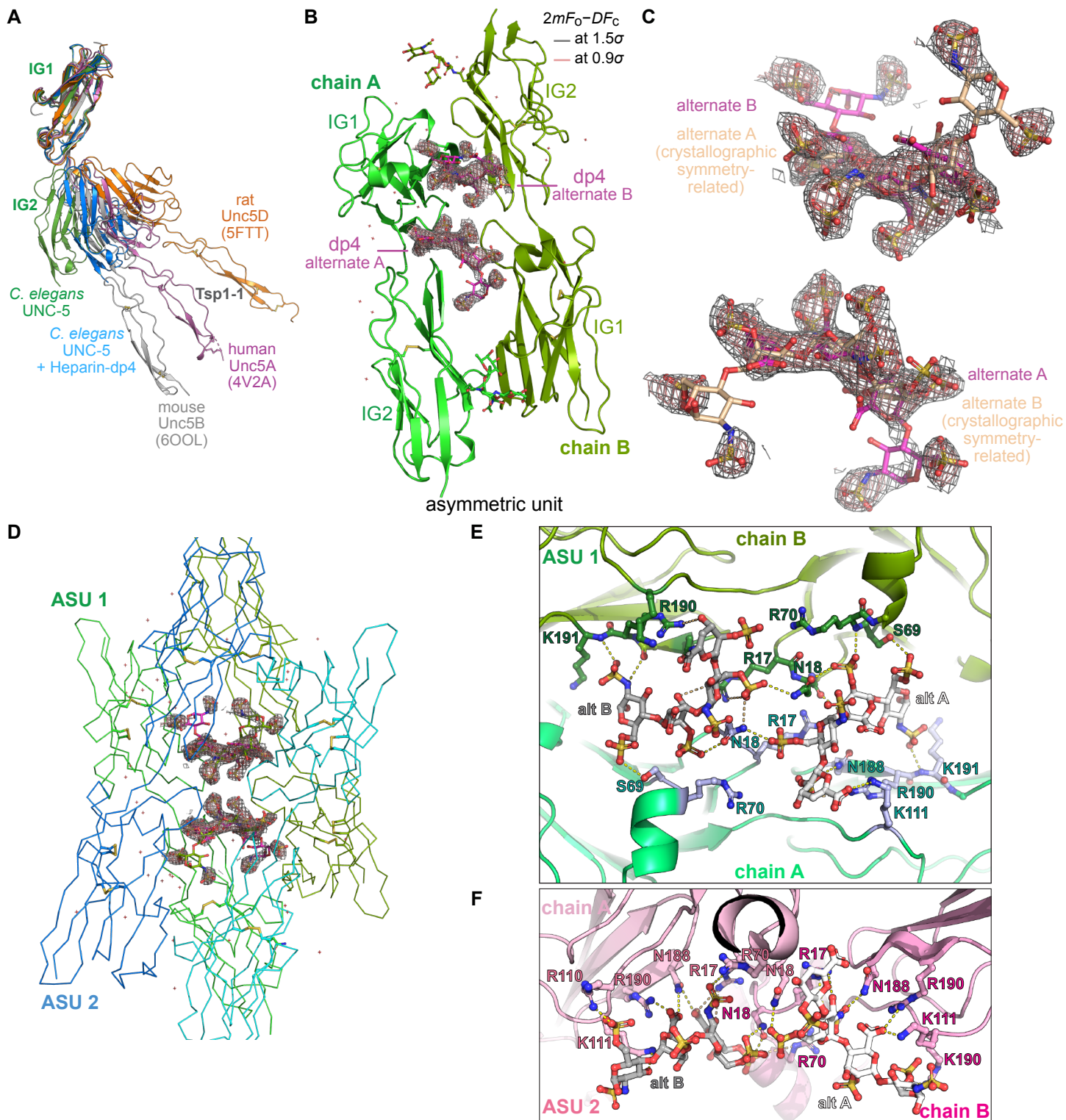


**Fig. S2. Electron density reveals the heparin-binding site on UNC-5.**

**A.** Superposition of reported UNC-5 structures in the literature and our UNC-5 IG1-2 structures, where the IG1 domains are overlaid, demonstrates wide flexibility of the IG1-IG2 boundary.

**B.** The asymmetric unit of the UNC-5-dp4 crystals, with  $2mF_o-DF_c$  density carved around the dp4 ligand. Heparin-dp4 was modeled as two alternate conformations in equivalent positions of the two UNC-5 chains related by non-crystallographic symmetry (light and dark green).

**C.** Electron density for heparin-dp4 with dp4 from two neighboring asymmetric units shown (colored magenta and salmon), each with two alternate copies. Density is strongest at the electron-rich sulfates.

**D.** Electron density for dp4 surrounded by four UNC-5 chains, contributed by two asymmetric units.

**E.** Close look at non-covalent interactions between dp4 molecules in both alternate conformations (alt A [white] and alt B [gray]) to two chains of UNC-5 in one asymmetric unit (ASU 1). Yellow and orange dashed lines are for polar interactions at  $\leq 3.5$  and at  $3.4$  to  $4$  Å, respectively.

**F.** Interactions of the same molecules to two UNC-5 chains in the next asymmetric unit (ASU 2).

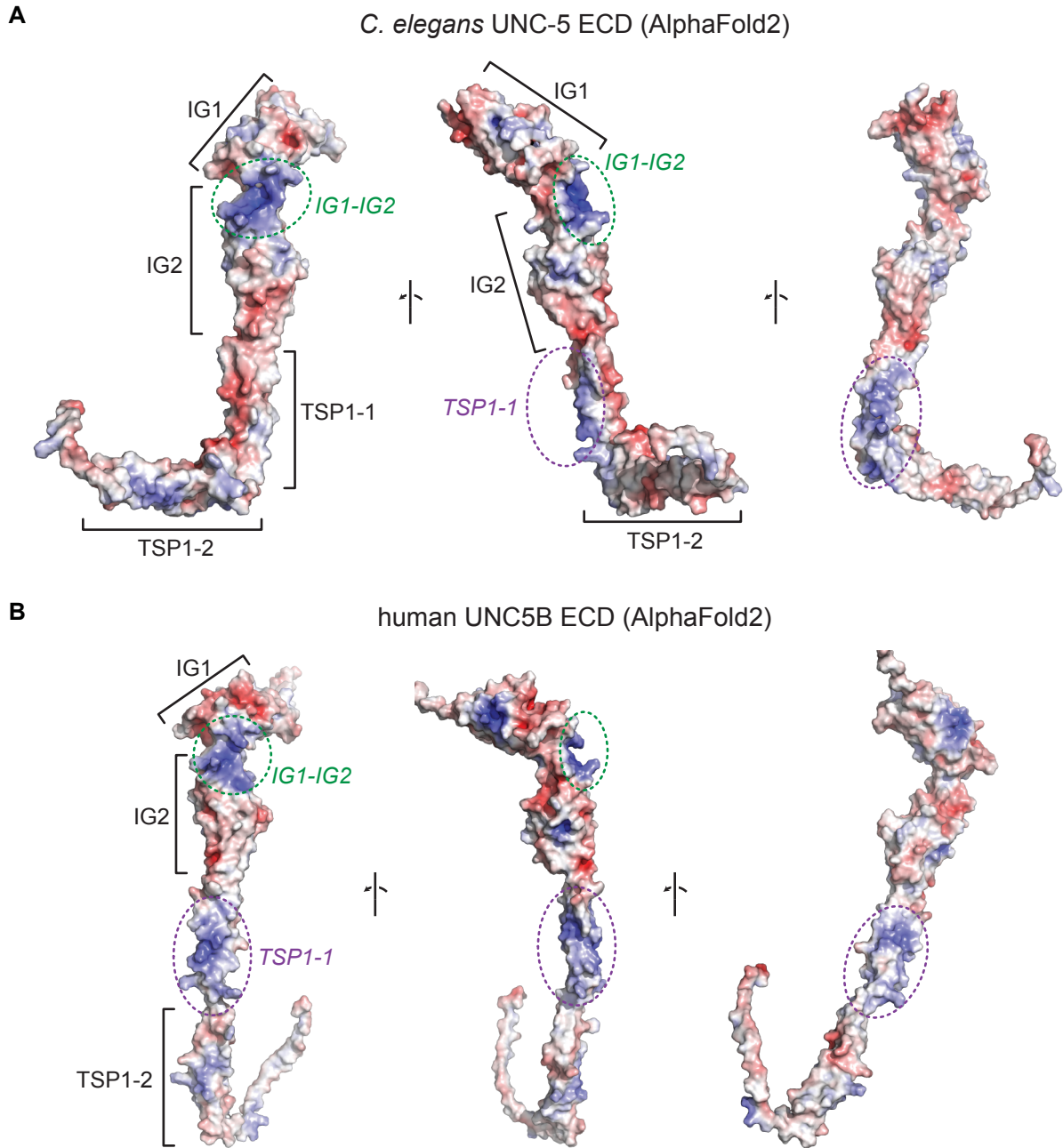


**Fig. S3. UNC-5 ectodomains have conserved positively charged surfaces.**

Electrostatic potential surfaces for *C. elegans* UNC-5 (A), and human UNC5B (B). Structural models for the entire ectodomains were taken from EBI's AlphaFold database. Both show positively charged surfaces on the IG1-IG2 boundary and on the first Tsp1 domain; however, the IG1-IG2 boundary is more conserved (Fig. 2G).

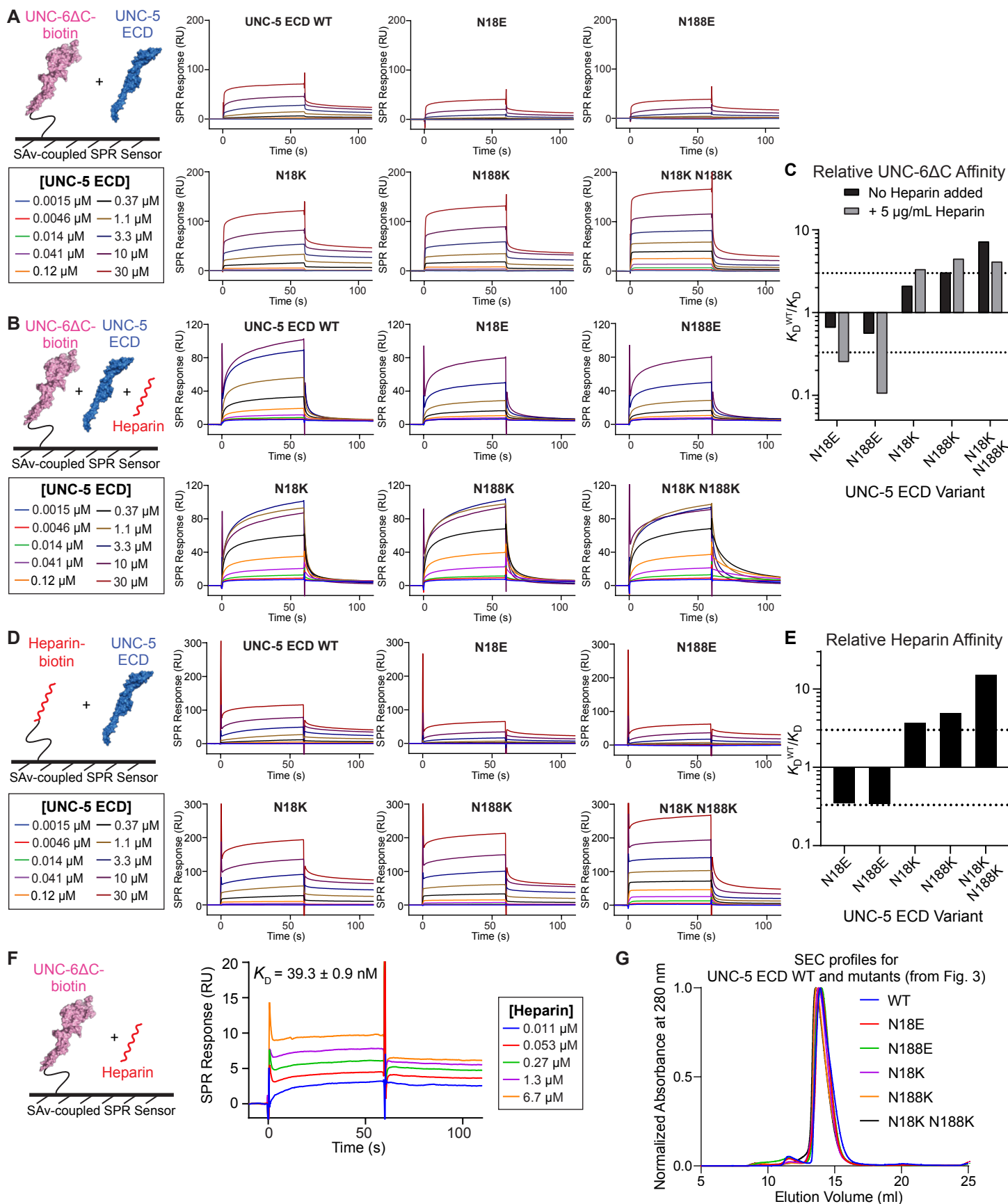


**Fig. S4. Mutations of UNC-5 N18 and N188 result in changes in heparin and UNC-6 affinity.**

**A,B,D,F.** SPR sensorgrams for isotherms reported in Fig. 3. Same channel on the SPR chip was used within each panel, allowing for direct comparison of response values between mutants. **C,E.** Loss or gain of UNC-6ΔC (C) or heparin (E) affinity for N18/N188 mutants of UNC-5 ECD, summarized as ratios of WT  $K_D$  to mutant  $K_D$ . **G.** SEC profiles for wild-type and N18/N188 mutants of UNC-5 ECD measured during purification over a Superdex 200 10/300 column.

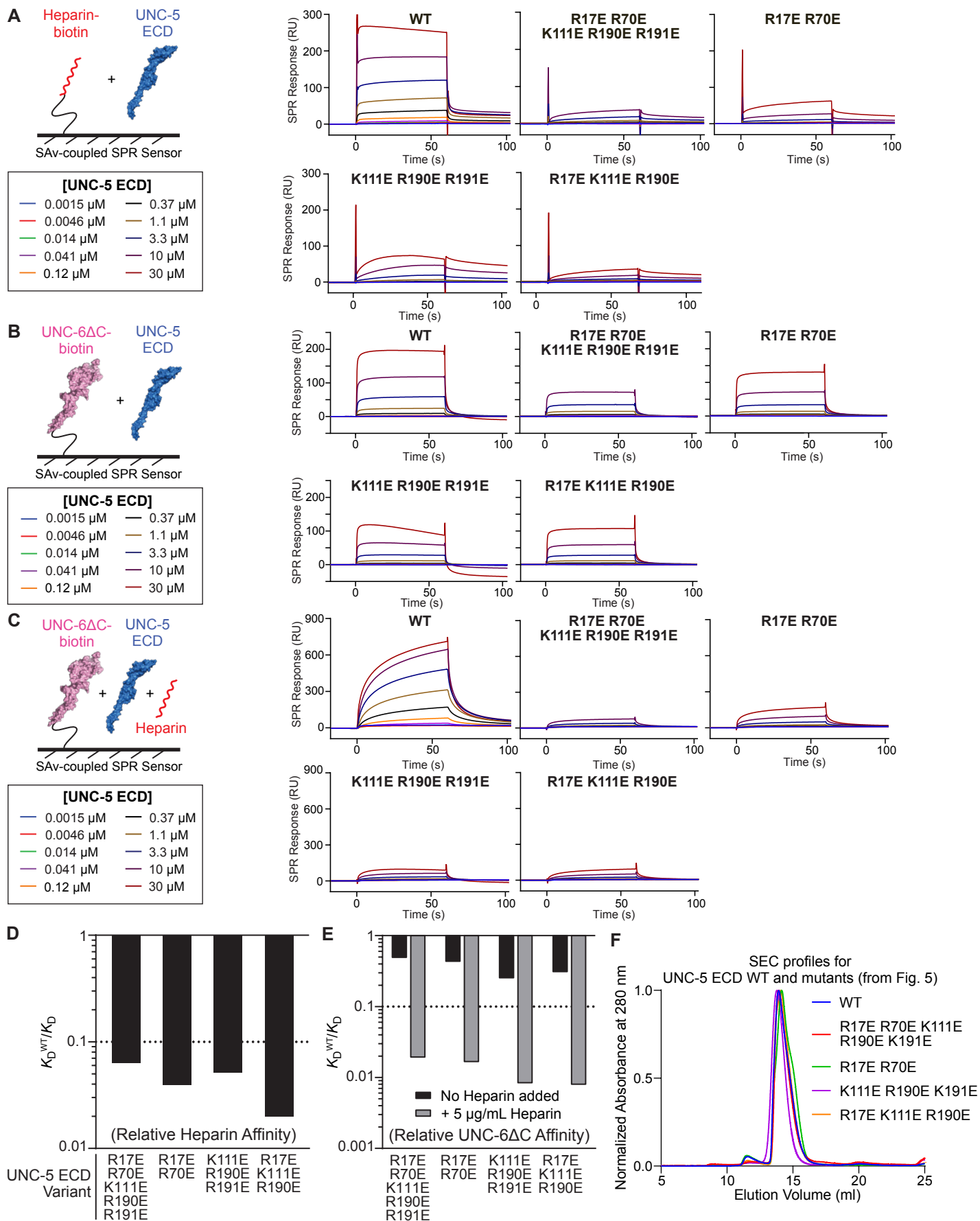


**Fig. S5. UNC-5 R/K→E mutations result in loss of heparin and UNC-6 affinity.** A-C. SPR sensorgrams for isotherms reported in Figure 4. Same channel on the SPR chip was used within each panel, allowing for direct comparison of response values between WT and mutants. D,E. Loss of heparin (D) and UNC-6ΔC (E) affinity of UNC-5 ECD R/K-to-E mutants, summarized as ratios of WT  $K_D$  to mutant  $K_D$ . Larger bars indicate larger loss of affinity. F. SEC profiles for wild-type and mutant UNC-5 ECD in panels A-C during purification over a Superdex 200 10/300 column.

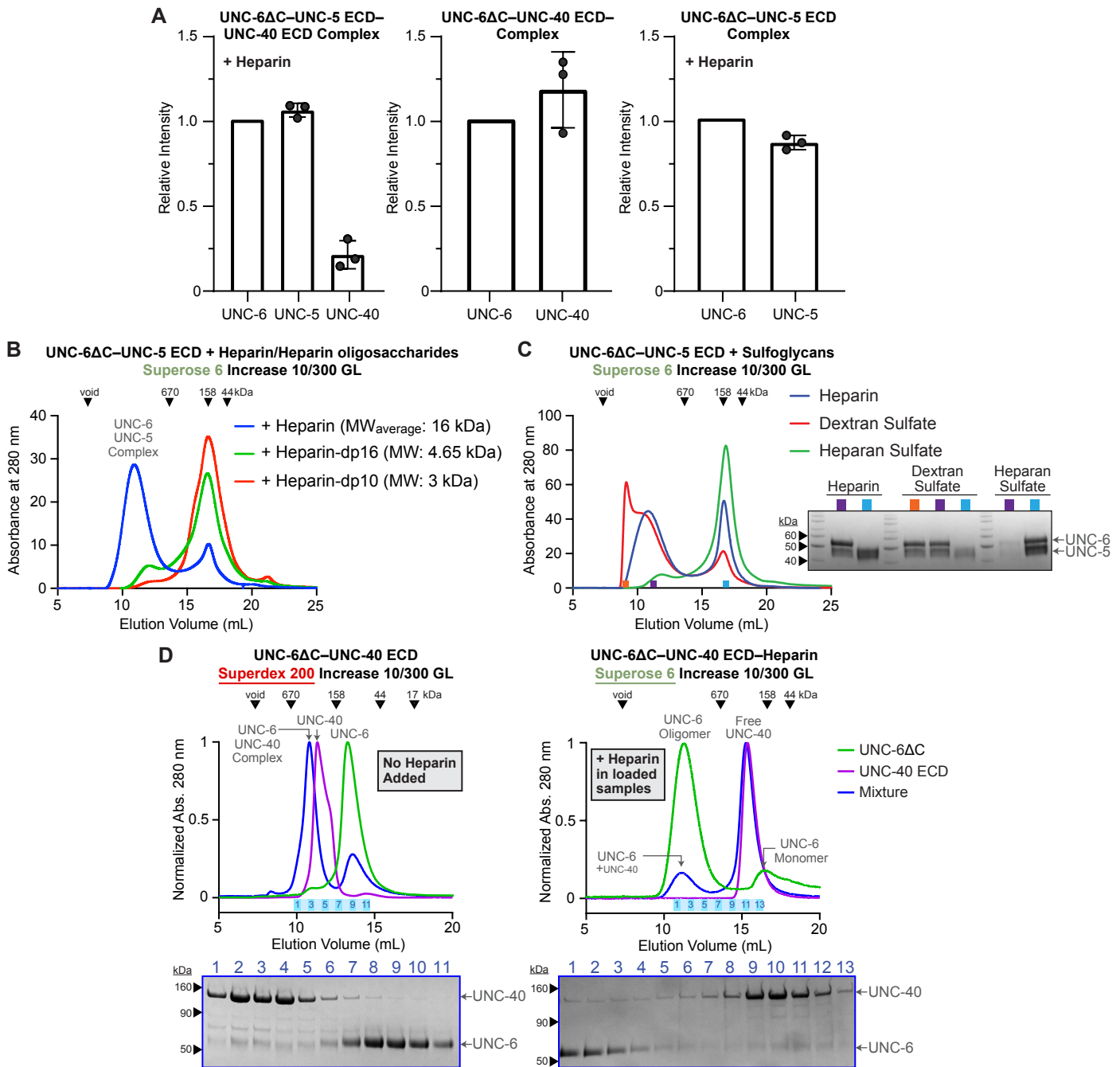


**Fig. S6. Sulfoglycans vary in their ability to promote large UNC-6ΔC-UNC-5 oligomers, while they exclude UNC-40 from these complexes.**

**A.** Coomassie blue-stained band intensities of purified UNC-6ΔC-UNC-5 ECD-UNC-40 ECD (Fig. 5B), UNC-6ΔC-UNC-40 ECD (Fig. 5C), and UNC-6ΔC-UNC-5 ECD (Fig. 5D) complexes were analyzed ( $n = 3$  lanes in SDS-polyacrylamide gels). All complexes were purified in SEC after mixing proteins in equimolar ratios, and with excess heparin (1.5 molar ratio) for the first two complexes. Band intensities were quantified using Image Lab (Bio-Rad Laboratories) and analyzed in Prism (GraphPad).

**B.** Long heparin chains are needed to create UNC-6-UNC-5 oligomers. Shorter heparin chains are less effective in complex formation, as assessed by SEC (Superose 6 Increase 10/300) (UV pathlength = 0.2 cm).

**C.** Formation of large UNC-6ΔC-UNC-5 ECD oligomers is more efficient with dextran sulfate and less efficient with heparan sulfate. UNC-6, UNC-5 and the sulfoglycans were mixed at 1:1:1.5 molar ratio.

**D.** (Left) SEC profiles for UNC-6ΔC, UNC-40 ECD, and 1.5:1 mixture of UNC-6ΔC:UNC-40 ECD ran on a Superdex 200 Increase 10/300 GL column. In the absence of heparin, most of the protein mixture forms an UNC-6ΔC-UNC-40 ECD complex and excess free UNC-6ΔC elutes later. (Right) SEC profiles for UNC-6ΔC, UNC-40 ECD, and 1:1:1.5 mixture of UNC-6ΔC:UNC-40 ECD:heparin ran on a Superose 6 10/300 GL column. When heparin is present in the protein mixture, the majority of UNC-6ΔC forms a high-MW oligomer with a substoichiometric amount UNC-40 ECD and excess free UNC-40 ECD elutes later. Please see that the two columns used on the left and right are different, since the complexes observed in the absence and presence of heparin are very different in size.

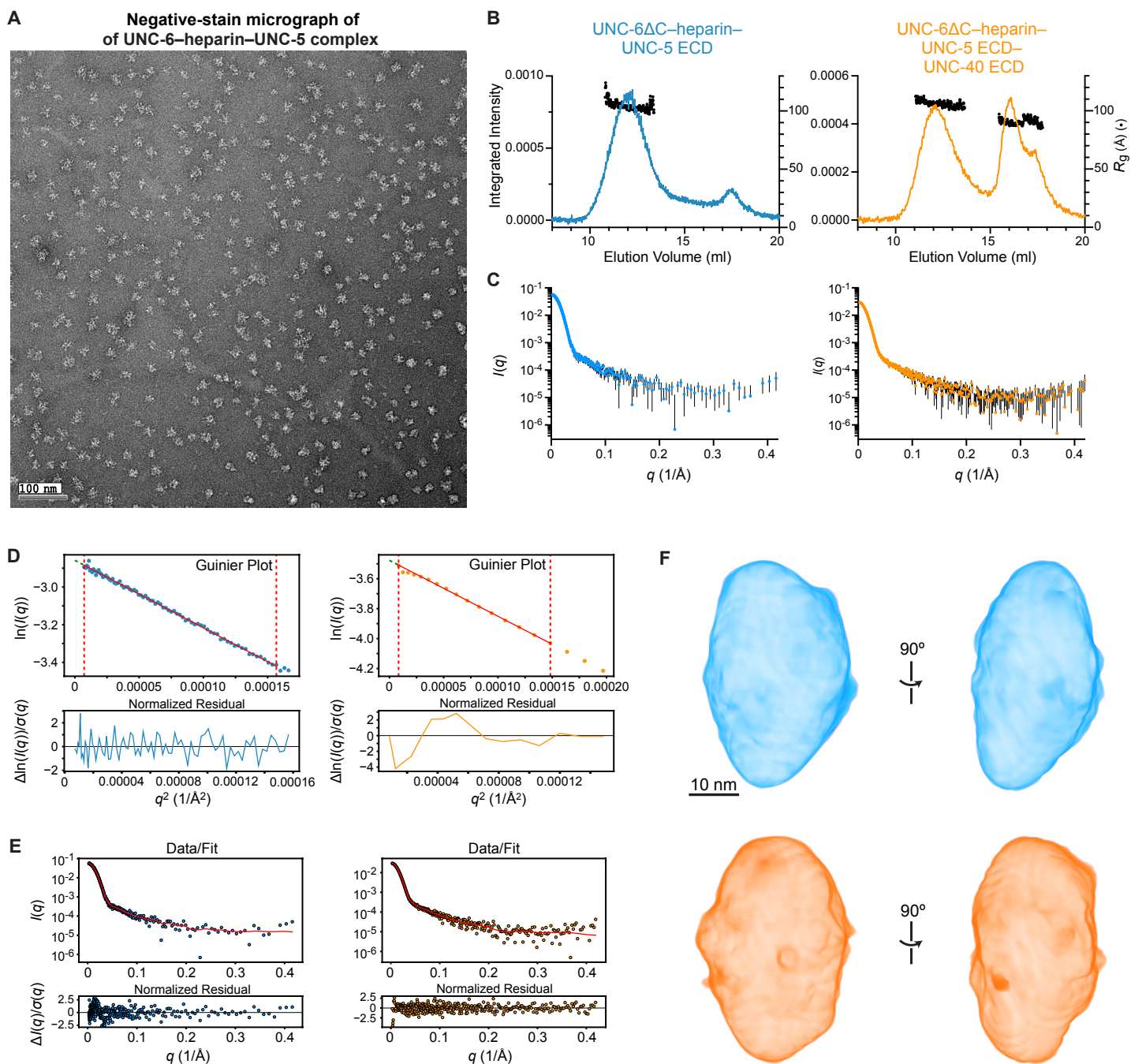


**Fig. S7. The UNC-6ΔC–UNC-5 ECD complex is globular and relatively rigid.**

**A.** Negative-stain EM micrograph of the UNC-6ΔC–heparin–UNC-5 ECD complex.

**B.** Integrated intensity profiles of SEC runs for SEC-SAXS data collected for the UNC-6 + heparin + UNC-5 (blue) and UNC-6 + heparin + UNC-5 + UNC-40 samples (orange), with radius of gyration ( $R_g$ ) overlaid on the peaks. A Superose 6 10/300 was used as the SEC column.

**C.** Scattering intensity as a function of scattering angle (transformed as the momentum transfer,  $q$ ) for the complex peaks.

**D.** The linear Guinier plot and the normalized residuals to the Guinier fits for both complexes.

**E.** The data fitting and residuals for the pair distribution plots in Fig. 5G for the UNC-6–heparin–UNC-5 complex (blue, left) and the UNC-6–heparin–UNC-5–UNC-40 complex (orange, right).

**F.** Volumes calculated for both complexes using DENSS.



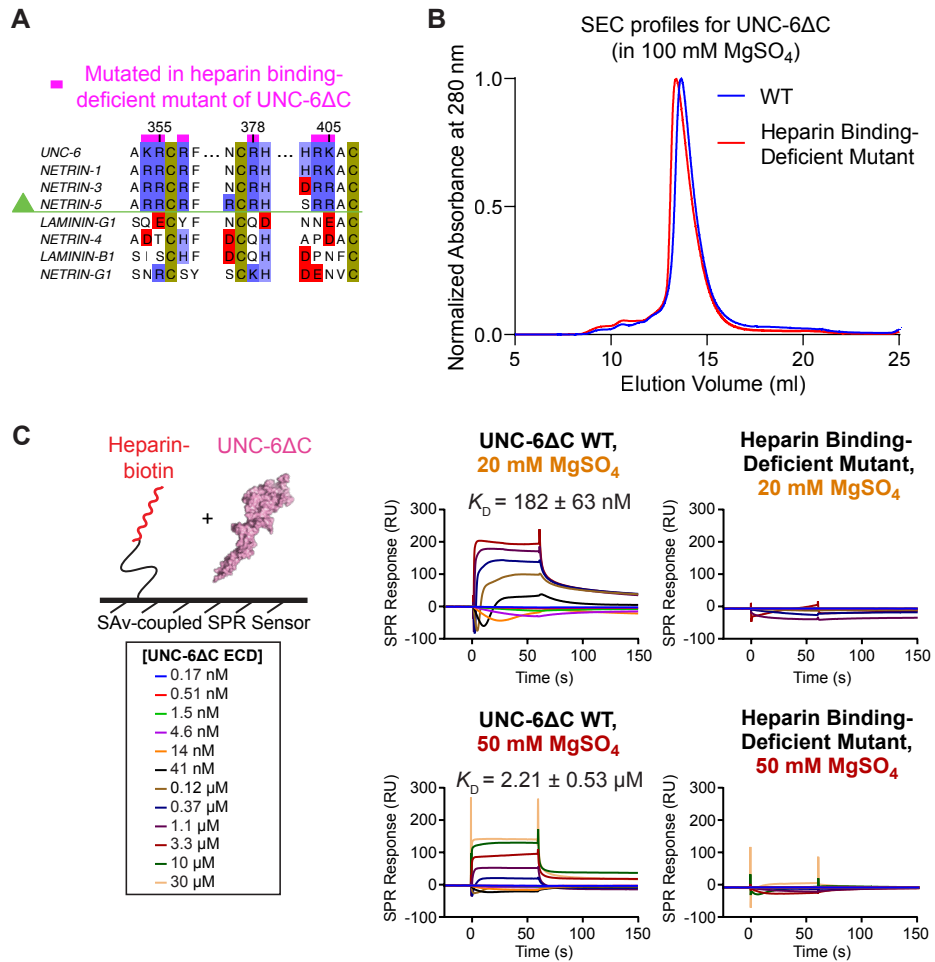


**Fig. S8. A closely related group within the Netrin family, including UNC-6 and mammalian Netrins-1, -3 and -5, have a conserved heparin-binding site on their EGF2 domain.**

**A.** Partial sequence alignment of UNC-6 and human Netrin homologs. UNC-6 and vertebrate Netrin-1, -3 and -5 evolved from a common ancestor, while Netrin-4 and Netrin-G1 have separate evolutionary origins.

**B.** SEC profiles for wild-type and mutant UNC-6ΔC used in SPR experiments in Fig. 6 during purification over a Superdex 200 10/300 column.

**C.** SPR sensorgrams for isotherms reported in Figure 6.

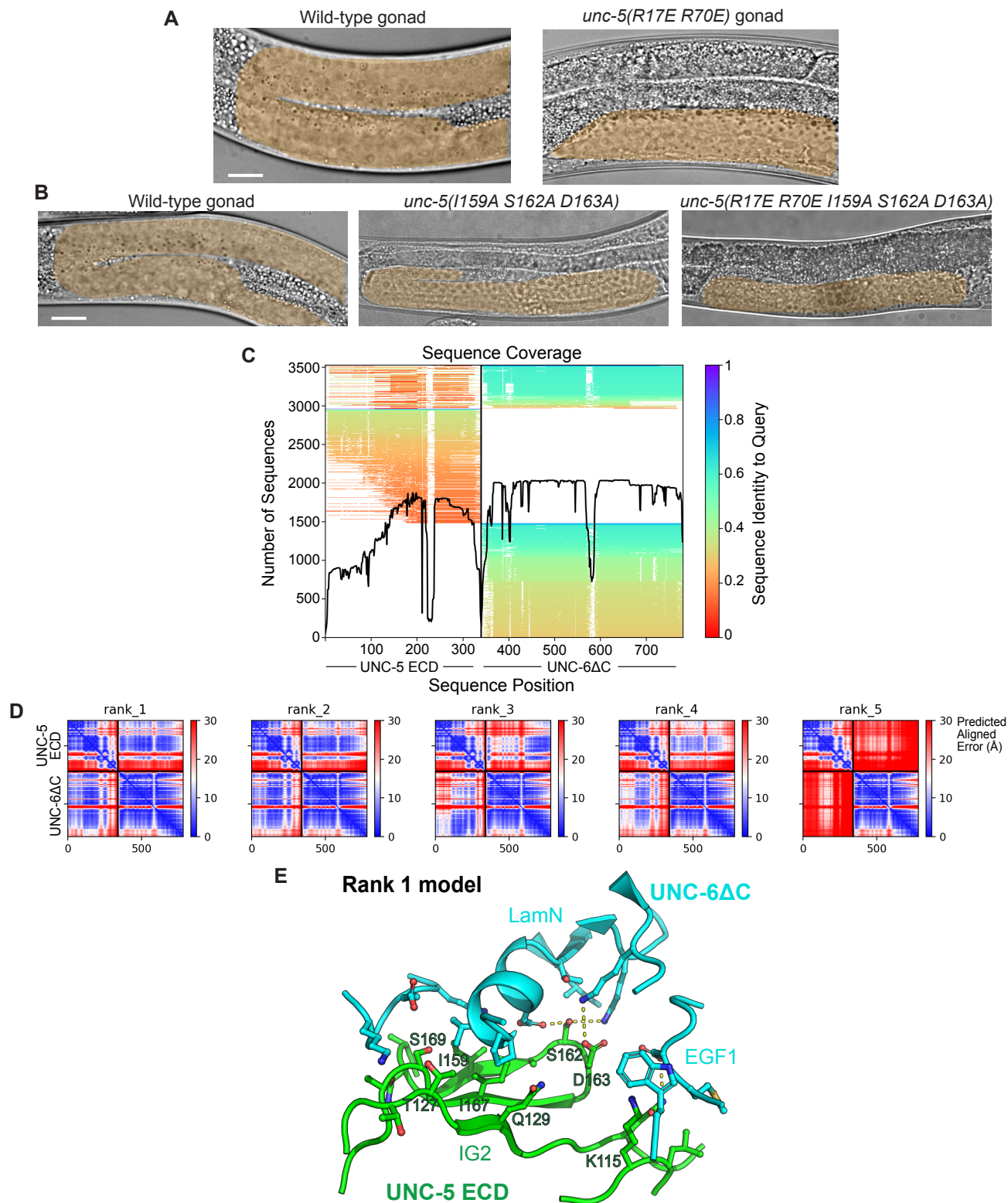


**Fig. S9. AlphaFold-multimer predicts an UNC-6–UNC-5 complex model with high confidence.**

**A,B.** Additional DIC images of gonad morphology in wildtype and engineered *unc-5* mutant animals. Yellow shaded area shows the gonad morphology. Scale bar is 10  $\mu$ m.

**C.** Statistics for the sequence alignment used in the AlphaFold prediction for the UNC-5 ECD–UNC-6 $\Delta$ C complex, including the number of sequences and sequence identity to query across the UNC-5 ECD and UNC-6 $\Delta$ C sequences.

**D.** Predicted Aligned Error values for five models predicted by AlphaFold. The best ranked (on the left) was used in designing interface mutants.

**E.** UNC-6–UNC-5 interface as predicted by AlphaFold (rank 1).

**Table S1.** Data and refinement statistics for x-ray crystallography.

	<i>C. elegans</i> UNC-5 IG1+2	<i>C. elegans</i> UNC-5 IG1+2 with Heparin-dp4	<i>C. elegans</i> UNC-6ΔC
<b>Data Collection</b>			
Beamline	ALS 8.2.1	APS 23-ID-B	APS 24-ID-E
Wavelength (Å)	0.9795	1.0332	0.9792
Space Group	C222	P6 <sub>1</sub> 22	P4 <sub>1</sub> 2 <sub>1</sub> 2
<i>Cell Dimensions</i>			
<i>a</i> , <i>b</i> , <i>c</i> (Å)	41.282, 130.216, 97.549	69.46, 69.46, 424.99	70.243, 70.243, 287.353
<i>α</i> , <i>β</i> , <i>γ</i> (°)	90, 90, 90	90, 90, 120	90, 90, 90
Resolution (Å)	50-2.89 (3.07-2.89)*	50-2.11 (2.30-2.11) <sup>†</sup>	200-2.5
<i>R</i> <sub>sym</sub> (%)	10.4 (85.5)	5.9 (166)	8.7 (216)
< <i>I</i> >/<σ( <i>I</i> )>	14.6 (1.9)	27.0 (2.0)	19.4 (1.3)
<i>CC</i> <sub>1/2</sub>	0.997 (0.722)	0.999 (0.724)	0.999 (0.700)
Completeness (%) (spherical)	98.6 (92.8)	58.0 (12.8) <sup>†</sup>	98.8 (98.3)
(ellipsoidal)	N/A	94.4 (82.2) <sup>†</sup>	N/A
Redundancy	5.1 (4.3)	18.4 (14.8)	13.1 (13.7)
<b>Refinement</b>			
Resolution (Å)	50-2.89 (3.18-2.89)*	50-2.11 (2.20-2.11)	68.23-2.50 (2.60-2.50)
Reflections	6,109	21,299	25748
<i>R</i> <sub>cryst</sub> (%)	24.59 (37.84)	24.02 (37.42)	22.00 (46.45)
<i>R</i> <sub>free</sub> (%)**	28.51 (42.57)	27.23 (53.73)	25.88 (55.15)
<i>Number of atoms</i>			
Protein	1511	3090	3188
Ligand/Glycans	48	216	95
Water	0	18	31
<i>Average B-factors (Å<sup>2</sup>)</i>			
All	73.0	68.1	88.7
Protein	72.1	67.5	88.1
Ligand/Glycans	102.1	78.8	117.6
Solvent	N/A	52.6	67.3
<i>R.m.s. deviations from ideality</i>			
Bond Lengths (Å)	0.002	0.010	0.008
Bond Angles (°)	0.418	1.178	0.899
<i>Ramachandran plot</i>			
Favored (%)	97.42	95.71	95.57
Outliers (%)	0.00	0.00	0.00
Rotamer Outliers (%)	0.00	0.29	0.84
All-atom Clashscore <sup>‡</sup>	4.58	7.15	4.24

\* The values in parentheses are for reflections in the highest resolution bin.

\*\* 10% of reflections (613) for UNC-5 IG1+2, 5% of reflections (1,065) for UNC-5 IG1+2 with dp4, and 5% of reflections (1,297) for UNC-6ΔC were not used during refinement for cross validation purposes.

<sup>†</sup> Diffraction limits (Å) and corresponding principal axes of the ellipsoid fitted to the diffraction cut-off surface as direction cosines in the orthogonal basis (standard PDB convention), and in terms of reciprocal unit-cell vectors, are:

Diffraction limit #1:	2.817 Å	(1.0000, 0.0000, 0.0000)	(0.894 <b>a</b> * - 0.447 <b>b</b> *)
Diffraction limit #2:	2.817 Å	(0.0000, 1.0000, 0.0000)	<b>b</b> *
Diffraction limit #3:	1.944 Å	(0.0000, 0.0000, 1.0000)	<b>c</b> *

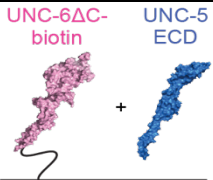
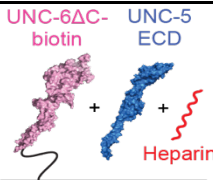
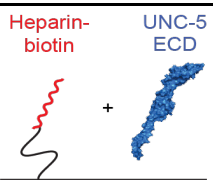
Eigenvalues of overall anisotropy tensor on |*F*|s (Å<sup>2</sup>) and corresponding eigenvectors of the overall anisotropy tensor as direction cosines in the orthogonal basis (standard PDB convention), and in terms of reciprocal unit-cell vectors:

Eigenvalue #1:	122.92	(1.0000, 0.0000, 0.0000)	(0.894 <b>a</b> * - 0.447 <b>b</b> *)
Eigenvalue #2:	122.92	(0.0000, 1.0000, 0.0000)	<b>b</b> *
Eigenvalue #3:	57.89	(0.0000, 0.0000, 1.0000)	<b>c</b> *

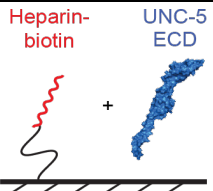
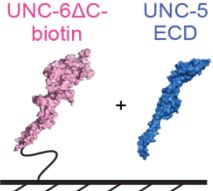
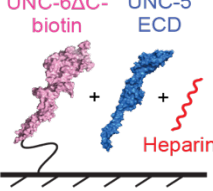
<sup>‡</sup> Clashscores were calculated by *phenix.refine* (PHENIX version 1.20).

N/A: Not applicable.

**Table S2.** Summary of fitting of SPR sensorgrams in Figure 4, with standard error of the parameter reported by Prism (GraphPad). Asterisks indicate maximum response was constrained during fitting of the isotherm, and therefore  $K_D$  estimates are less accurate.

Experimental Design	UNC-5 ECD variant	$K_D$ ( $\mu\text{M}$ )	Standard error of the fit ( $\mu\text{M}$ )	$K_D^{\text{WT}}/K_D$
 <p>UNC-6ΔC-biotin + UNC-5 ECD</p> <p>SAV-coupled SPR Sensor</p>	Wild-type	45.7*	1.4	1.00
	N18E	70.9*	1.5	0.645
	N188E	83.7*	7.5	0.546
	N18K	21.3*	1.0	2.15
	N188K	14.7*	0.8	3.12
N18K N188K	6.20	0.56	7.38	
 <p>UNC-6ΔC-biotin + UNC-5 ECD + Heparin</p> <p>SAV-coupled SPR Sensor</p>	Wild-type	1.17	0.05	1.00
	N18E	4.70*	0.12	0.248
	N188E	11.3*	0.5	0.103
	N18K	0.341*	0.069	3.41
	N188K	0.255*	0.038	4.57
N18K N188K	0.277*	0.053	4.21	
 <p>Heparin-biotin + UNC-5 ECD</p> <p>SAV-coupled SPR Sensor</p>	Wild-type	26.3*	3.6	1.00
	N18E	78.9*	4.7	0.334
	N188E	80.8*	6.6	0.326
	N18K	6.84*	0.78	3.85
	N188K	5.14*	0.54	5.12
N18K N188K	1.68	0.36	15.7	

**Table S3.** Summary of fitting of SPR sensorgrams in Figure 5, with standard error of the parameter reported by Prism (GraphPad). Asterisks indicate maximum response was constrained during fitting of the isotherm, and therefore  $K_D$  estimates are less accurate.

Experimental Design	UNC-5 ECD variant	$K_D$ ( $\mu\text{M}$ )	Standard error of the fit ( $\mu\text{M}$ )	$K_D^{\text{WT}}/K_D$
 <p>SAV-coupled SPR Sensor</p>	Wild-type	3.86	0.34	1.00
	R17E R70E K111E R190E R191E	62.3*	3.3	0.0620
	R17E R70E	100*	3	0.0385
	K111E R190E R191E	77.0*	8.8	0.0502
	R17E K111E R190E	197*	11	0.0196
 <p>SAV-coupled SPR Sensor</p>	Wild-type	12.8	0.2	1.00
	R17E R70E K111E R190E R191E	27.1*	0.9	0.473
	R17E R70E	30.8*	1.1	0.416
	K111E R190E R191E	52.5*	5.1	0.244
	R17E K111E R190E	43.0*	2.1	0.298
 <p>SAV-coupled SPR Sensor</p>	Wild-type	1.44	0.11	1.00
	R17E R70E K111E R190E R191E	77.6*	10.9	0.0186
	R17E R70E	89.6*	8.1	0.0161
	K111E R190E R191E	178*	25	0.00809
	R17E K111E R190E	187*	17	0.00768

**Table S4.** Data collection details and analysis for multi-angle light scattering experiments.

	<b>UNC-5 ECD + UNC-6ΔC + heparin</b>	<b>UNC-5 ECD + UNC-6ΔC + UNC-40 ECD + heparin</b>
Experiment Type	SEC-MALS-SAXS	
Instrument	DAWN HELEOS with Optilab T-rEX at BioCAT (APS beamline 18-ID)	
Wavelength (nm)	663 (for light scattering) and 658 (for RI)	
Flow rate (ml/min)	0.6	
Chromatography column	Superose 6 10/300 Increase	
Buffer	10 mM HEPES pH 7.2, 150 mM NaCl, 100 mM MgSO <sub>4</sub>	
Refractive index of the solvent (assumed)	1.321	
Temperature	25°C	
Software	ASTRA version 7 (Wyatt)	
Loading volume (μl)	450	300
Loading concentration (mg/ml)	0.89 (complex mixture)	1.09 (complex mixture)
<i>dn/dc</i> *	0.188 for protein including N-glycans 0.133 for heparin	0.188 for protein including N-glycans 0.133 for heparin
Extinction coefficient at 280 nm	1.139 ml/(mg×cm)	1.145 ml/(mg×cm)
<i>M<sub>n</sub></i> **	1,980,000 (±0.12%) Glycoprotein: 1,605,000 Conjugate (Heparin): 375,000	1,590,000 (±0.11%) Glycoprotein: 1,304,000 Conjugate (Heparin): 286,000
<i>M<sub>w</sub></i> †	1,997,000 (±0.12%) Glycoprotein: 1,634,000 Conjugate (Heparin): 363,000	1,596,000 (±0.11%) Glycoprotein: 1,316,000 Conjugate (Heparin): 280,000

\* *dn/dc* values are estimated based on predicted N-linked glycosylation content.

\*\* Number-averaged molar mass.

† Weight-averaged molar mass.

**Table S5.** Data statistics and analysis for small angle x-ray scattering experiments.

	UNC-5 ECD + UNC-6ΔC + heparin	UNC-5 ECD + UNC-6ΔC + UNC-40 ECD + heparin
<i>Data Collection and Sample Details</i>		
Experiment setup	SEC-MALS-SAXS	SEC-MALS-SAXS with co-flow during SAXS
Instrument	BioCAT facility at APS beamline 18-ID with Eiger2 XE 9M detector	
Wavelength (Å)	1.033	1.033
Camera length (m)	3.654	3.682
$q$ -measurement range (Å <sup>-1</sup> )	0.0027 to 0.42	0.0027 to 0.42
Exposure time (s)	0.25	0.5
Exposure period (s)	1.0	1.0
Flow rate (ml/min)	0.6	0.6
Chromatography column	Superose 6 10/300 Increase	
Buffer	10 mM HEPES pH 7.2, 150 mM NaCl, 100 mM MgSO <sub>4</sub>	
Temperature	22°C	22°C
Software	BioXTAS RAW version 2.1.4, ATSAS 3.1.3	
Loading concentration (mg/ml)	0.89	3.0
Loading volume (μl)	450	300
<i>Structural Parameters</i>		
Guinier Analysis*		
$I(0)$ (cm <sup>-1</sup> )	0.0574 ± 0.00011	0.0309 ± 0.00005
$R_g$ (Å)	103.72 ± 0.49	105.85 ± 0.25
$q$ range (Å <sup>-1</sup> )	0.00268 to 0.01252	0.00291 to 0.01218
$q_{\min}R_g$ to $q_{\max}R_g$	0.2778 to 1.2987	0.3075 to 1.2891
Coefficient of Correlation, $R^2$	0.9975	0.9958
$P(r)$ Analysis (from GNOM**)		
$I(0)$ (cm <sup>-1</sup> )	0.0577 ± 0.00011	0.0310 ± 0.00005
$R_g$ (Å)	105.30 ± 0.06	106.60 ± 0.26
$D_{\max}$ (Å)	373	365
$q$ range (Å <sup>-1</sup> )	0.0027 to 0.4157	0.0029 to 0.419
$\chi^2$	1.1127	0.8835
Molecular Weight Estimates		
Vc method***	2.48 MDa	2.33 MDa
Vp method†	1.33 MDa	1.77 MDa
Shape & Size method‡	1.08 MDa	1.07 MDa

\* Performed in BioXTAS RAW (76).

\*\* By Svergun (78).

\*\*\* By Rambo and Tainer (79). This method may not work well with mixed (protein with conjugate) samples.

† By Piiadov, et al. (80). This method may not work well with non-protein samples.

‡ By Franke, et al. (81). This method may not work well with non-protein samples.